Incorporation of Smart Concrete in Large-Scale RC Beams for Evaluating Self-Sensing and structural Properties

Arvind Kumar Cholker[1] 📷

Abstract

Only using a small number of samples in the absence of reinforcement, the concrete self-monitoring behaviour is tested, which is inaccurate for real-world structures. The behaviour of concrete is primarily tested, which can be inaccurate for structures in real time. This study examined the self-sensing ability of large-scale reinforced concrete beams that are 1500 mm long and 125 mm wide embedded with smart concrete at top and bottom surfaces for a length of 350 mm. As shear failure is catastrophic, the present study focused on evaluating RC beams' self-sensing property failing under shear, and shear reinforcement was not given for the same reason. A total of six RC beams, 3 of are 250 mm deep and 3 are 350 mm deep with variable reinforcement ratios, were tested in a four-point bending test to study the self-sensing properties such as strain and crack/damage sensing. Mechanical/structural properties of all the beams have been documented, along with self-sensing properties. The results obtained showed that partially placed smart concrete in the RC beam's pure bending region successfully sensed all strain and damage/cracks without any impact due to beam depth and reinforcement ratio. During testing, it was observed that 250-mm-deep beams failed due to flexure/concrete crushing, and 350-mm-deep beams failed due to shear. In particular, smart concrete's self-sensing property showed promising results for the beams that failed due to flexure by representing all the cracks developed in the pure bending region. Fraction change in resistance (FCR) has also been obtained for all the beams during self-sensing testing, and this FCR has been successfully co-related with concrete strain in compression and steel strain in tension. An empirical equation was also derived separately for beams that failed in shear and flexure, which provides a co-relation between FCR and concrete or steel strain.

Keywords Smart concrete · Carbon fibres · Health monitoring · Electrical properties · Flexural properties

1 Introduction

The fact that concrete is the most widely used substance on Earth, after water, is well known. The designed environment comprises massive, complex, and costly structural systems that are constructed with concrete. While catastrophic failures can be avoided by following the structural design codes when in service, infrastructures eventually face destruction. Failure/damage of the structure may be caused for many reasons, such as mechanical loads, earthquakes, dimensional change of structural element due to creep/shrinkage, environmental loads or freezing/thawing effect, and change in temperature or combination of those types of loads. It is necessary to detect and repair any structural damage as early as possible to maintain the infrastructure in a serviceable condition.

The method of implementing a damage identification and characterisation strategy for engineering structures like buildings or bridges is referred to as structural health monitoring (SHM). The SHM technique is presently used to detect any damage in the structure, rather than on visual inspection alone, as visual inspection is subjective and labour-intensive [1]. Usually, SHM is a process in which sensors like strain gauges, electrochemical sensors, optical fibre sensors, shape memory alloys, piezoelectric ceramics, and conductive polymer composites are embedded/installed on a concrete surface, and data recorded using a sensor are collected at a server station that is far from the site. Collection of these data from site to server room needs a large number of cable wires that need to be installed, resulting in high system cost, difficulty in mass production,

✉ Arvind Kumar Cholker
  arvind_06phd16@nitsri.net

1 National Institute of Technology Srinagar, Srinagar, India

and labour-intensive again. For instance, it requires 10–15 sensors at the cost of $5000 per sensor channel for a small-scale system [2]. Therefore, if we follow the same for large buildings or bridges with long spans, it becomes very costly, as they need more sensors in number [3, 4]. Besides, considering the availability of sensors and their SHM usability [5, 6], for continuous monitoring, most sensors are stated to be non-durable, uneconomical, inaccessible, and ineffective with concrete structures [7]. It is essential to overcome these disadvantages to ensure widespread implementation and sustainability.

Therefore, one possible solution to solve the aforementioned demerits is to create a concrete that can sense external loads, vibrations, strains, etc. without compromising strength. This type of concrete is named as a self-sensing concert and can be produced by incorporating any electrically conductive materials (ECMs) like carbon fibres/nanofibrers [8–10], carbon tubes (single- or multi-walled)/nanotubes [1, 11–16], single carbon black [17–19], bucky paper [20], nickel powder, and graphene [21, 22]-like materials within the concrete body homogeneously so that they form continues electrical network. The addition of these conductive materials to concrete imparts sensing ability as it shows a change in electrical properties (i.e. resistivity) when loaded/disturbed externally. Also sensing concrete has absolute friendly compatibility and an equal lifetime compared with other smarter sensors used in SHM due to its cement-based property when embedded within concrete structures. Furthermore, along with SHM, sensing concrete exhibits substantially improved safety, mechanical properties, durability, serviceability, and reliability of the infrastructures over standard concrete due to functional filler reinforcement [23]. In addition to the above-said advantages, self-sensing concrete can be used for traffic monitoring to obtain Traffic parameters, like traffic vehicular speed, traffic density, flow rates, and vehicle classification. The aforesaid multiple applications of smart concrete are due to its self-sensing property and easiness to manufacture in any shape and size for fulfilling various engineering applications.

In the literature, studies focusing on the dispersion and mixing methods of the above-mentioned ECMs in a cement matrix, the effect of ECMs on mechanical strength and self-sensing property individually or in combination, the dosage quantity of ECMs, and the effect of curing period on sensing can be identified [24–30]. Wen and Chung [31] researched the effects of embedded steel reinforcement on self-sensing concrete, in addition to the above considerations on self-sensing. Results showed that these embedded steel reinforcement bars positively affect the Piezoresistive behaviour of carbon fibre-based composites under flexural loading. It is noted from the current literature review that the study on smart concrete/self-sensing concrete is limited to cement composites and concrete cubes. Therefore, the authors decided to examine the relationship between electrical properties and structural properties of reinforced concrete (RC) beams under flexural loading, and thus to monitor structures in the everyday world.

In the present study, the primary focus during the four-point bending test was on self-sensing properties and shear failure of large-scale RC beams, as shear failure is catastrophic. The current research consists of producing and testing six large-scale RC beams with varying depths and reinforcement ratios embedded with chopped carbon fibres under four-point bending tests. Compared to other types of carbon material, carbon fibres were selected based on the authors' positive results in the recent study [7, 32]. Mechanical and structural properties are also reported, along with the self-sensing properties of the large-scale RC beam.

2 Experimental Details

2.1 Test Specimens

A total of six simply supported RC beams were built and tested with a constant bending region under four-point loading. Out of 6 beams, three beams were of 250 mm depth, and 3 were of 350 mm depth. For all the beams, a constant length of 1500 mm and width of 125 mm was maintained. Since the research was focused on self-sensing and shears failure, no reinforcement was provided for the shear and compression zone. All the beams were therefore supported only with passive tension-side reinforcement with differing diameters in different beams. Table 1 and Fig. 1 present the detailing

Table 1 Properties of testing beam

S. no	Beam designation	Grade of concrete	b/mm	d/mm	A_{st}	$\rho s/\%$
1	M2-A-250	21.3	125	250	2–10Φ	0.502
2	M2-B-250	21.5	125	250	2–10Φ, 2–8Φ	0.824
3	M2-C-250	21.1	125	250	2–8Φ, 2–8Φ	0.643
4	M2-A-350	21.3	125	350	2–16Φ	0.92
5	M2-B-350	21.5	125	350	2–16Φ, 2–12Φ	1.43
6	M2-C-350	21.1	125	350	2–12Φ, 2–12Φ	1.02

Fig. 1 Beam detailing
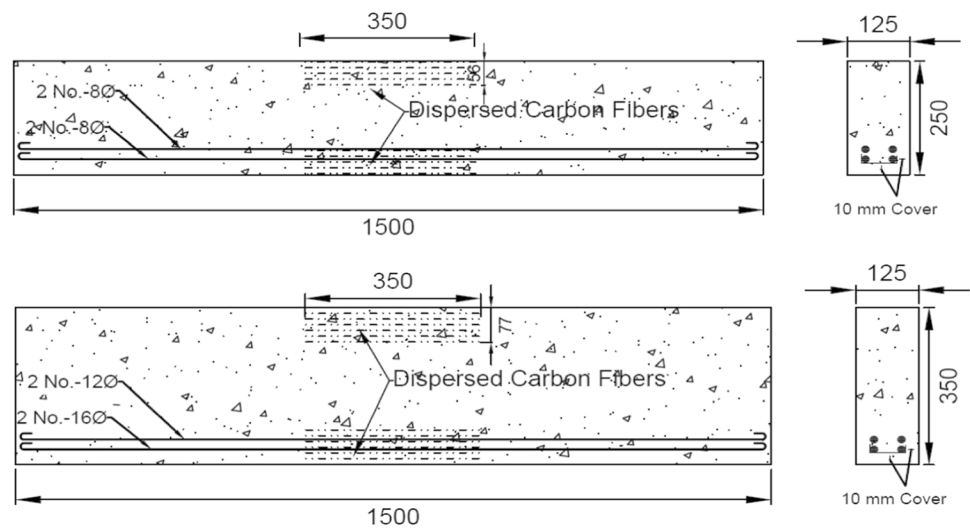
Table 2 Mix proportion for SCC

S. no	Materials used	Quantity/m^3 of concrete (kgs)	Remarks
1	Cement (PC-43 grade)	445	With compressive strength 43 N/mm2
2	Fine aggregate	786	Zone-III and FM-2.56
3	Water ready admixture	6.75	PCE-based superplasticiser
4	Coarse aggregate (10 mm)	853	FM-6.88
5	Surfactant	0.32	SDBS
6	Carbon fibre	7.425	Electrically conductive fibres
7	Water	188.1	Tap water with pH 7.1

FM fineness modulus, *SDBS* dedocyl benzene sulphonic acid sodium salt

of all the beams. For convenient purposes, each beam was indicated using numbers and letters. For example, in beam M2-A-350, numeral 350 represents the depth of the beam, letter A represents reinforcement ratio, and M2 represents the grade of concrete which was constant for all the beams.

2.2 Materials, Proportioning, and Mixing

SCC mix with adequate performance was chosen to manufacture RC beams after conducting several test mixes on self-compacting concrete (SCC). The selected SCC mix had both plastic flow capacity as per EFNARC [33] and required strength in the hardened state [34]. For SCC production, Portland cement, locally available coarse aggregates with a maximum size of 10 mm, and zone II fine aggregates with a specific gravity of 3.15, 2.74, and 2.69 were used, respectively. In addition to the water-cement ratio of 0.38, a high-range water reducer was used to achieve a uniform distribution of fibres and concrete flow. The blended proportions of materials adopted for the production of self-sensing concrete and self-compacting concrete in the current study are shown in Table 2.

Table 3 Material properties of reinforcement

Steel type	d_s/mm	A_s/mm^2	f_y/MPa	f_u/MPa	E_s/GPa
Longitudinal reinforcement	8	50.2	617.2	717.7	200
	10	78.5	540	658.8	201
	12	113	690	771.9	200
	16	201	545	687.1	198

Steel moulds were used to cast RC beams, and the corresponding concrete cubes were also cast from regular 150 mm steel moulds for each beam to check their compressive strength. After 24 h, all specimens were demoulded and placed in the water tank for 28 days for curing. HYSD longitudinal bars whose features are given in Table 3 have been used in the present study. Carbon fibres (CF) of type SYC-TR-PU were added to the concrete mix with a cement weight of 1.5%, the properties of which are shown in Table 4 [35]. Based on the findings obtained by the author [36], the 1.5 percent dosage of carbon fibres by cement weight was selected as it forms the threshold level.

Table 4 Carbon fibre properties

Carbon content	%	95
Tensile strength	MPa	4,810
Electrical resistivity	w.cm	1.54×10^{-3}
Elongation	%	2.3
Tensile modulus	GPa	225
Density	g/litre	1.78
Filament diameter	μm	6.97
Length	Mm	6

2.2.1 Smart Concrete

In the present study, concrete embedded with carbon fibre, i.e. self-sensing/smart concrete (carbon fibre-based concrete), was only positioned in the midsection at the bottom. A top surface for a 350 mm fixed length and a depth of 56 mm for a beam depth of 250 mm and 77 mm for a beam depth of 350 mm has to be checked under pure bending as shown in Fig. 1. Since the beam is subjected to maximum compressive strain and tensile strain on the top and bottom surface, CFs were only introduced to that section from an economic point of view, retaining the ratio of smart concrete depth to beam depth as 0.22. The purpose of adding carbon fibre is to investigate the strain, damage-sensing property of RC beam upon loading, and analyse the pattern of correlation between the electrical properties and structural properties of RC beam so that it can be used for health monitoring of a structure/building remotely.

Production of smart/self-sensing concrete and self-compacting concrete used for manufacturing of beams was done simultaneously but in different mixers. The main difference between self-compacting concrete (SCC) and smart concrete is carbon fibres in smart concrete. For the production of smart concrete with a uniform distribution of CFs, initially, a solution of water and surfactant was prepared to disperse fibres in water with the surfactant's help. CFs (of the required amount) were added to this obtained solution. Further blending was carried out for ten minutes using a manufactured mechanical churner that resulted in a random but uniform distribution of fibres in the water. In a concrete mixer, this uniformly dispersed fibre solution was then progressively applied to dry cement, coarse aggregates, and fine aggregates and blended until the necessary flow was obtained by adding a superplasticiser the development of smart concrete in a fresh state. For the 350-mm-deep beam, the newly produced smart concrete was positioned using a separate smaller middle steel mould (350 mm deep, 125 mm wide, and 350 mm long) in the beam's central portion. Firstly, at the necessary depth of 77 mm, the middle steel mould was filled with smart concrete, followed by the addition of SCC to the main beam (bigger) mould and also to the
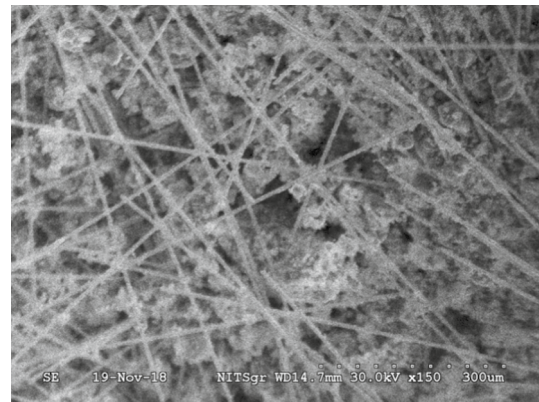

Fig. 2 SEM image of dispersed carbon fibre

smaller mould. SCC was added in the smaller mould only to the height from which it required the remaining top portion of the smart concrete. After the RC beam's failure, the fibre distribution in hardened concrete was analysed using a scanning electron microscope (SEM), and the SEM image is shown in Fig. 2. Figure 2 shows that carbon fibres were uniformly distributed in the concrete that was needed for the production of smart concrete.

3 Test Procedure and Instrumentation

Each beam was tested to failure under a four-point bending test to investigate the effect of micro-carbon fibre on self-sensing and the effect of depth and reinforcement on self-sensing. The load was gradually applied to the beam using a hydraulic jack with a capacity of 50 tonnes, and load recording was done using a load cell of 500 kN capacity attached to the hydraulic jack. Midspan deflection, change in length at the upper, and bottom beam surface in the pure bending region were measured using LVDTs. The length of the LVDT used for measuring compressive strain in concrete was 25 mm (Useful electrical stroke), and the length of the LVDT used for measuring beam deflection was 100 mm both having the least count of 0.01 mm, displacement speed ≤ 10 m/s, and displacement force ≤ 4 N. Figure 3 shows the complete test set-up. Strain in the beam reinforcement was obtained using strain gauges attached to steel bars during casting of the beam. All the experimental readings were automatically recorded using a data logger.

Change in electrical resistance at the upper and lower surface of smart concrete in the pure bending region was recorded using two different digital multimeters (DMMs). Initially, electrically conductive paint was applied to the RC beam at the inside face of the load application point at the top surface and opposite it in the bottom surface for recording electrical resistance readings of smart concrete. Copper

(a) Schematic view of the test configuration
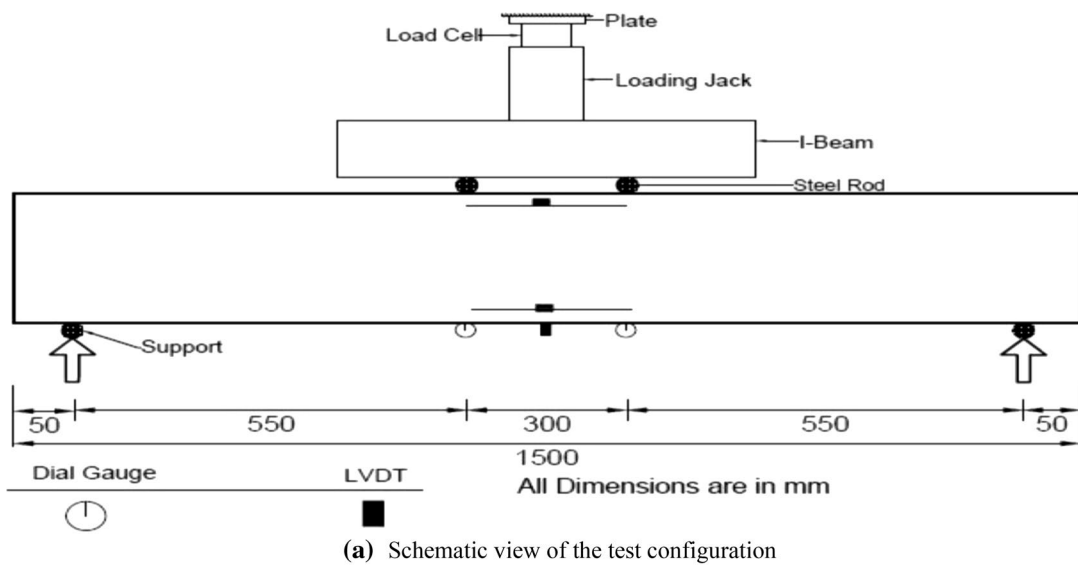
(b) Photograph of the experimental setup

Fig. 3 Experimental set-up view

wires connected to DMMs were stuck to this conductive paint with the aid of adhesive tape to ensure perfect bonding and continuous readings. Besides, to record and store readings, these data logger and DMMs were linked to the PC. The portrayal of the entire instrumentation is depicted in Fig. 4.

4 Experimental Results and Discussions

4.1 Electrical Investigation

4.1.1 Initial Electrical Resistance

The initial surface resistance was assessed before loading on the RC beam's upper and lower surfaces to confirm the existence of embedded smart concrete. From the obtained results shown in Fig. 5, it can be seen that the initial resistance is in kilo-ohms which is needed for self-sensing concrete.
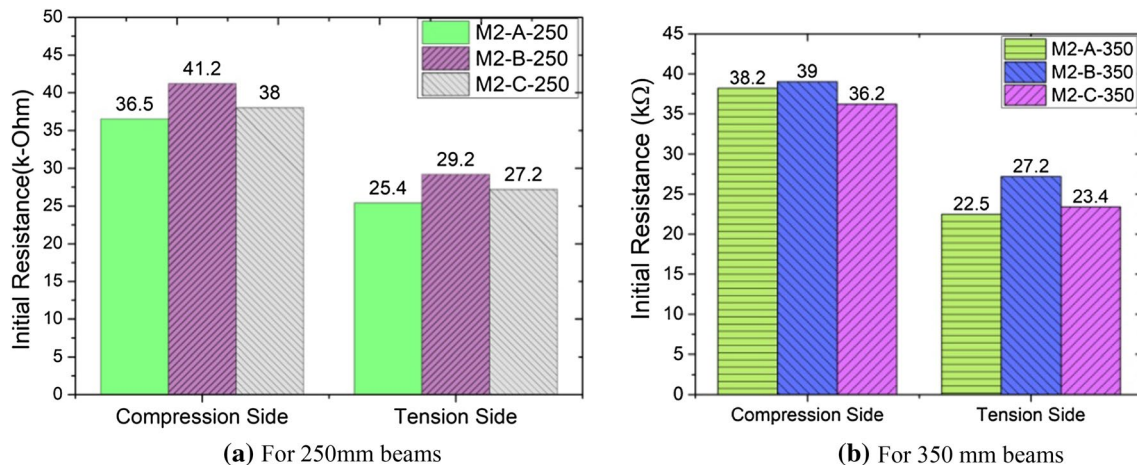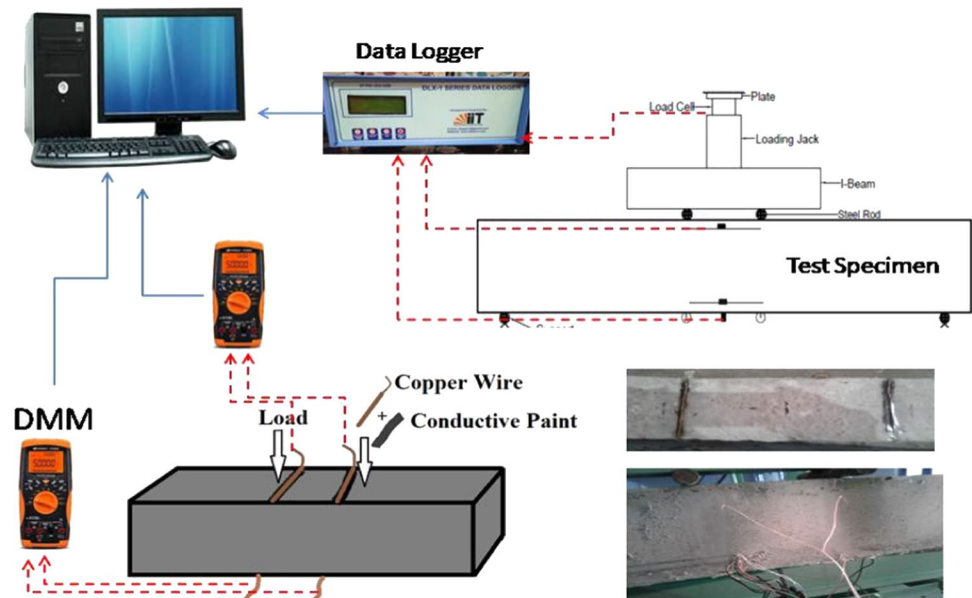
Fig. 4 Instrumentation of test set-up

Fig. 5 Initial electrical resistance of the top and bottom surface

(a) For 250mm beams

(b) For 350 mm beams

Studies reported that the addition of ECMs in conventional concrete reduces its electrical resistivity from giga-ohms to kilo-ohms. The initial surface resistance of smart concrete found in the current study is between 22.5 and 41.2 k-Ohm, which can be considered very effective for external load sensations. It is also observed that the initial surface resistance is lower on the tension side compared to the compression side regardless of the steel reinforcement ratio for both sets of beams. This is because the RC beam's piezoresistivity was improved by the presence of steel bars at the tension side, which wen and Chung also observed [31]. It is important to note that the presence of different diameter steel bars (reinforcement ratio) in 250 mm and 350 mm beams did not affect the initial resistance a lot. Therefore, the reinforcement ratio and depth of the beam do not affect the initial

resistance of self-sensing concrete. The initial surface resistance observed at the compression surface is between 36.5 and 38 k-Ohms for the tensile surface and 25.4–29.2 k-Ohms for the 250 mm beam surface. Similarly, for a 350-mm-deep beam, the initial compression surface resistance is between 36.2 and 38.2 k-Ohms and 22.5–27.2 k-Ohms for the tensile surface.

4.1.2 Compressive Strain and FCR

The load was applied progressively during RC beam testing until beam failure. Electrical resistance changes were recorded separately on the surface of tension (bottom) and compression (top) using two separate DMMs during loading in the pure bending region. Using beam-mounted

LVDT, the compressive concrete strain was recorded, and the tensile strain was recorded using strain gauges attached to reinforcement.

Experimental measurements of electrical resistance yielded an FCR value calculated using Eq. (1). Figure 6 displays the plot of obtained FCR values for both the compression and the tension side concerning the time from initial loading to beam failure. It was found that, regardless of the depth and reinforcement ratio, all beams have been shown to decrease the FCR and concrete compressive strain with increased load. The potential explanation for the decrease in FCR is that the compression length (top) surface decreases during loading, so that carbon fibres present in the smart concrete push towards each other, resulting in less electrical resistance or electrical conductivity.

$$FCR = \frac{\Delta R}{R_0} = \frac{R - R_0}{R_0} \qquad (1)$$

The FCR plot was found to decrease in a linearly in curved manner for all the beams, regardless of the reinforcement ratio and beam depth, as the load increased to the point of crack formation. In the case of beams with a depth of 250 mm, the FCR plot was found to be curvilinear and showed abrupt changes following crack formation in the concrete. This abrupt change in the FCR plot was due to the formation of cracks in the top concrete surface and the crushing of concrete due to compression. There was a substantial difference in resistance at the failure stage in the case of beam M2-B-250, and it was also found that after the beam's failure, the fractional change in resistance increases again. This is because the

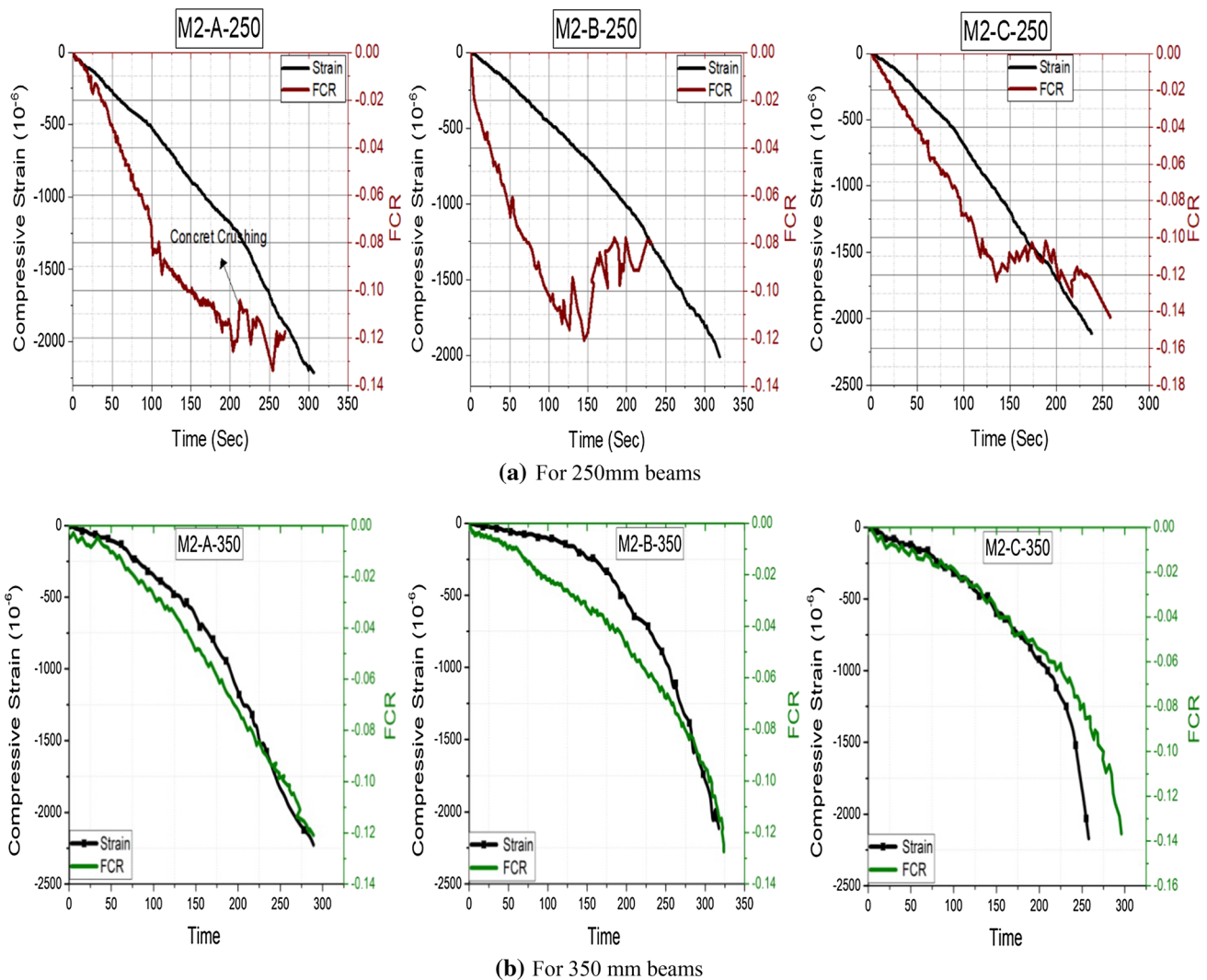
(a) For 250mm beams

(b) For 350 mm beams

Fig. 6 Plot of FCR and compressive strain

beam collapsed due to concrete crushing, resulting in an increase in electrical resistance due to the creation of gaps in smart concrete within carbon fibres that resulted in electrical charges being discontinued.

On the other hand, the fractional change in resistance in beam M2-A-250 and M2-C-250 was continuously decreasing up to the beam's failure, adumbrating that the failure of the beam was due to the yielding of steel rather than concrete crushing. On the other hand, for 350-mm-deep beams, the FCR plot was marginally smoother and increased in the curvilinear form before beam failure. Since all 350-mm-deep beams had no cracks on the top concrete surface, the FCR curve followed a monotonic and curvilinear pattern until the final failure as the ultimate failure was caused by shear.

4.1.3 Tensile Strain and FCR

The reinforcement stain and FCR plot on the bottom surface under tension are shown in Fig. 7. It was noteworthy that the FCR graph pattern for the surface of tension was quite contrary to that of the surface of compression. The FCR plot and reinforcement strain increased linearly as the load increased until the beam crack was formed. It was found that, regardless of the depth and reinforcement ratio in the beam, the pattern was very similar. As load increases, the tensile strain in reinforcement and FCR increased for all the beams, and there was abrupt growth in the FCR graph at the time of flexural crack formation. This unexpected rise in the FCR plot was again attributed to discontinuity in the smart concrete due to crack formation, lowering electrical charge flow, and increasing resistance. The sudden increase and continuity in tension
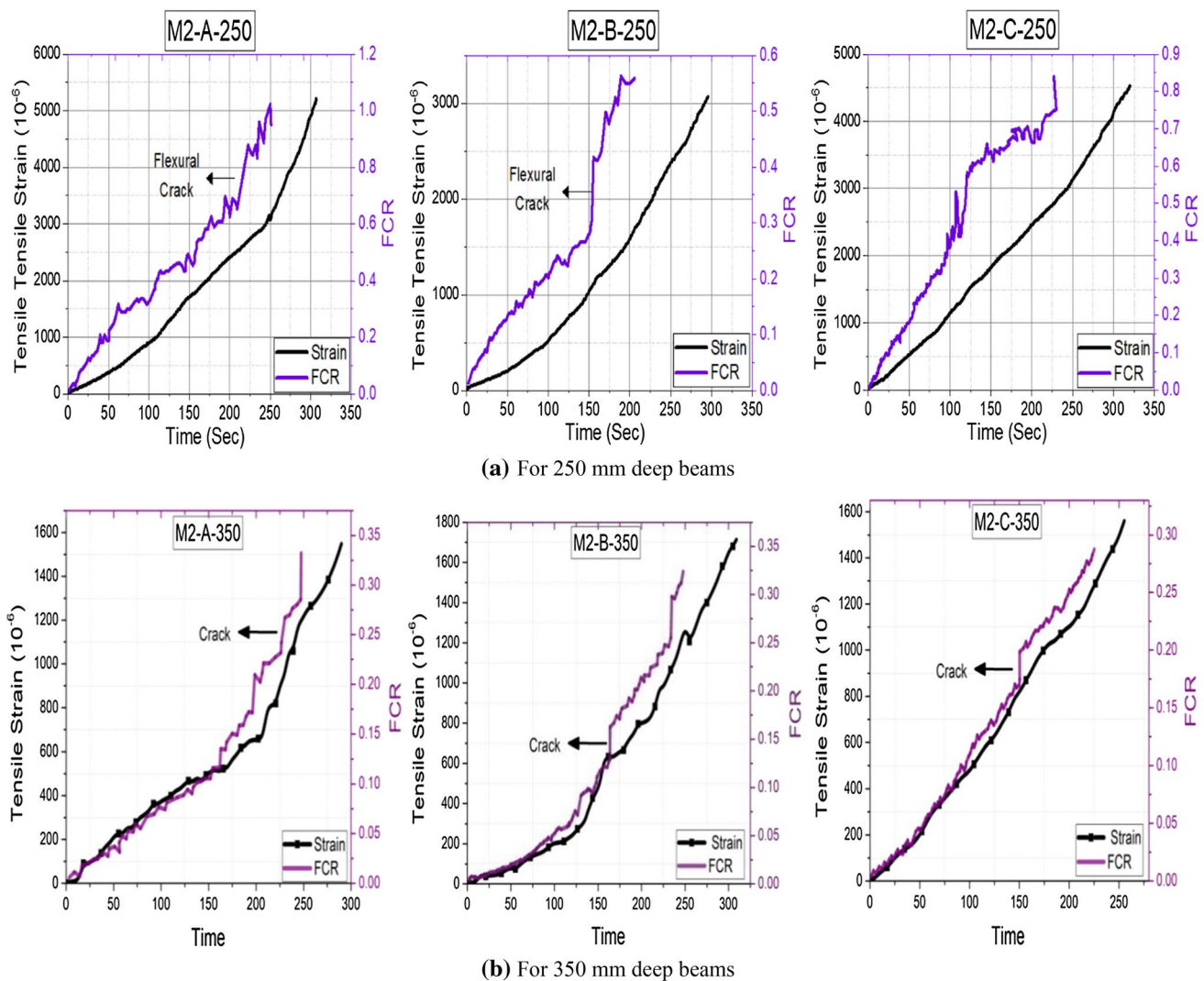

(a) For 250 mm deep beams

(b) For 350 mm deep beams

Fig. 7 Tensile strains in reinforcement and FCR at tension (bottom) surface

surface FCR plot in all the beams indicate the formation of micro-crack at that instance during tension surface loading, offering a new structural health monitoring method that can be used to find/sense cracks/damage in an RC beam. The greater the number of sudden increases in the FCR plot, the greater the number of cracks produced. There was an immediate increase in the FCR plot by creating a wider crack due to the complete breakage of the electric charge flow path. FCR differed continuously at the tension surface for beams M2-A250 and M2-C-250, relative to beam M2-B-250, which was due to the creation of numerous cracks at various loading levels and ultimate failure was due to reinforcement yield. On the other side, beams with 350 mm depth showed a smooth linear increment plot of FCR during loading with fewer flexural cracks as an ultimate failure for all 350-mm-deep beams was due to shear. It can therefore be said that the strain in concrete can be found with FCR values of carbon fibre-based concrete (smart concrete) and also detect the crack formation that gives a new approach of SHM that does not use any external or integrated sensors such as strain gauges/LVDTs/infrared cameras, etc.

4.1.4 Gauge Factors of Smart Concrete

A method called the gauge factor (GF) can be used to calculate the sensitivity of smart concrete/carbon fibre concrete strain and can be defined as a proportion of fractional resistance change (FCR) and unit strain in the concrete [17, 18]. In the present study, GF is calculated using Eq. (2).

$$\text{GF} = \frac{\left(\Delta R | R_0\right)}{\Delta \varepsilon} = \frac{\left(\Delta R | R_0\right)}{\left(\varepsilon_{\text{pc}} - 0\right)} \tag{2}$$

The comparative gauge factor values of all the beams have been calculated using the above equation and are shown in Fig. 8. From the obtained results, it was observed that GF at the compression side was less compared to the tension side and ranged between 58 and 199 and was much higher than that of the commercially conventional gauge factor involving metal (approximately 2). This is probably because of the presence of reinforcement that increased strain sensing sensitivity of the smart concrete at the tension side. The difference between GFs for beams of 250 mm and 350 mm depth was negligible, indicating that the loading rate was the same for both beams during testing. Similar growth in GFs (enhanced damage-sensing property) was observed by Nguyen et al. [37] when macro-steel fibre-reinforced concrete (MSFRCs) was embedded with 0.5 vol.% micro-carbon fibres.

4.2 Structural Behaviour

As carbon fibres were introduced for structural health monitoring in the reinforced concrete beam, it is imperative to study these carbon fibres' effect on structural properties such as shear capacity, ultimate moment carrying capacity, RC beam stiffness/ductility, and deflection. For the same reason, all the beams were tested for four-point loading, and it was observed from the results obtained that all the beams initially showed flexural cracking in the constant bending region, but for different beams, the ultimate failure was different. The
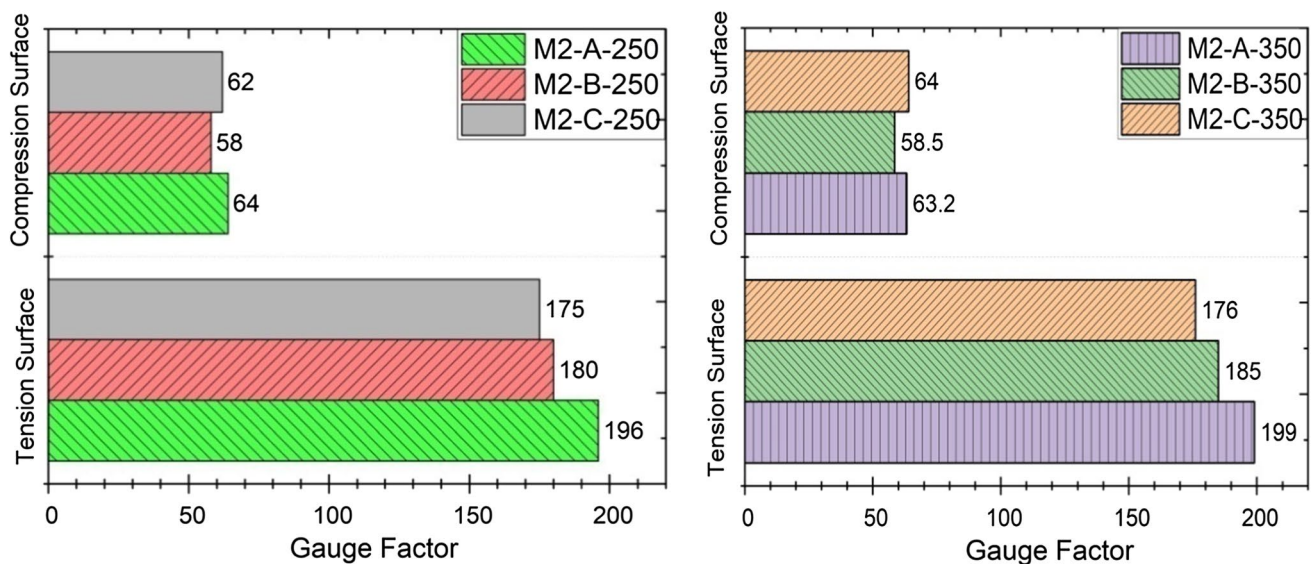

Fig. 8 GFs for of smart concrete at compression and tension side

complete structural behaviour of all the beams is discussed in detail below.

4.2.1 Failure Pattern of RC Beams

Tables 5 and 6 summarise the essential parameters of the experimental findings, and Fig. 9 shows a comparison of the beam cracking pattern. It was noted during testing that while both 250-mm- and 350-mm-deep beams initially showed flexural crack at low applied loads in the midspan region, the ultimate failure of beam M2-B-250 was due to concrete crushing at the compression surface. However, in the pure bending region, some minor shear cracks initiated, there is no shearing force, but it is due to the little shearing produced by the beam's self-weight. Finally, these cracks merged with the flexural cracks that led to ultimate failure. Beams M2-A-250 and M2-C-250 with reinforcement ratios of 0.50 and 0.64 also showed flexural cracks at the initial stage, but ultimate failure was due to yielding reinforcement. The probable reason for concrete compression in the beam M2-B-250 is the presence of a higher reinforcement ratio (0.82) that made the beam stronger at the tension side than the concrete strength.

On the other side, as depth increased from 250 to 350 mm, the ultimate failure was due to shear rather than concrete crushing or yielding of reinforcement. During testing, it was observed that at low applied loads all the 350-mm-deep beams showed micro-flexural cracks at initial loading in the pure bending region. But as load increased further, new diagonal micro-cracks formation took place in shear span zone at tension surface, and with further increment in loading, these micro-cracks got wider and ultimate failure was due to shear. This is probably due to higher reinforcement without shear stirrups that caused shear failure to make diagonal crack predominant.

4.2.2 Effect of Longitudinal Reinforcement Ratio

From the load–deflection curves shown in Fig. 10, it is found that the reinforcement ratio has a significant role in the load–deflection response, the ultimate load-carrying capacity, and the stiffness. It is noted in the series of 250 mm beams that the lower reinforcement ratio beam (M2-A-250) showed more deflection before failure. The ultimate deflection decreases as the percentage of reinforcement ratio increased, and the beam M2-B-250 with a higher reinforcement ratio failed abruptly without showing much deflection. Because of the rise in the flexural reinforcement ratio, the deflection was decreased, which induced an increase in the moment of inertia (flexural stiffness), resulting in a decrease in displacement at the same amount of load. An increase in reinforcement ratio increased the ultimate moment carrying capacity of the beam within a specific limit of deflection as also observed by Abdoladel Shoaib [38]. It was also noticed that the final moment carrying potential of the beam improved with an improvement in the reinforcing ratio for 250-mm-deep beams. The obtained experimental ultimate moment (Mu-exp) values for M2-A-250, M2-B-250, and M2-C-250 beams are 17.93 kN-m, 21.89 kN-m, and 19.38 kN-m, respectively.

It can be seen from the load–deflection plot of 350-mm-deep beam that the load-carrying capacity of the beam increased as the reinforcement ratio increased for a constant grade of concrete. It can also be observed from the same plot that there was no reinforcement yield in either of the beams as the beam failed suddenly due to shear. It is noteworthy that as the depth of the beam increased from 250 to 350 mm, there was an improvement in deflection. It was found that beam deflection decreased at the same load levels for 350 mm beam depth and had much lower deflection before failure compared to 250 mm beam deflection.

Table 5 Summary of test results for 250-mm-deep beams

Beam designation	Ultimate state		Flexural cracking		Yielding state		Ultimate moment	Ductility index	
	P_u/kN	Δu/mm	P_{cr}/kN	Δcr/mm	P_y/kN	Δy/mm	$M_{u(exp)}$/(kN-m)	$\Delta u/\Delta cr$	$\Delta u/\Delta y$
M2-A-250	64.54	10.05	40.24	3.60	62.30	5.40	17.93	2.79	1.86
M2-B-250	79.60	7.46	51.20	3.90	69.80	5.10	21.89	1.91	1.46
M2-C-250	70.48	9.53	43.20	3.62	64.00	4.80	19.38	2.63	1.98

Table 6 Summary of test results for 350-mm-deep beams

Beam designation	Ultimate state		Initial shear cracking load	Exp. shear	Normalised shear	Failure
	P_u/kN	Δu/mm	V_{cr} (kN)	V_{exp}, (kN)	$V_{exp}/\sqrt{f'c}bd$,(Mpa)	
M2-A-350	77.88	2.03	52.3	38.94	0.22	DTF
M2-B-350	110.5	4.94	95.3	55.26	0.31	DTF
M2-C-350	82.40	3.58	66.4	41.2	0.23	DTF

Fig. 9 Crack pattern in test beams

M2-A-250

M2-B-250

M2-C-250

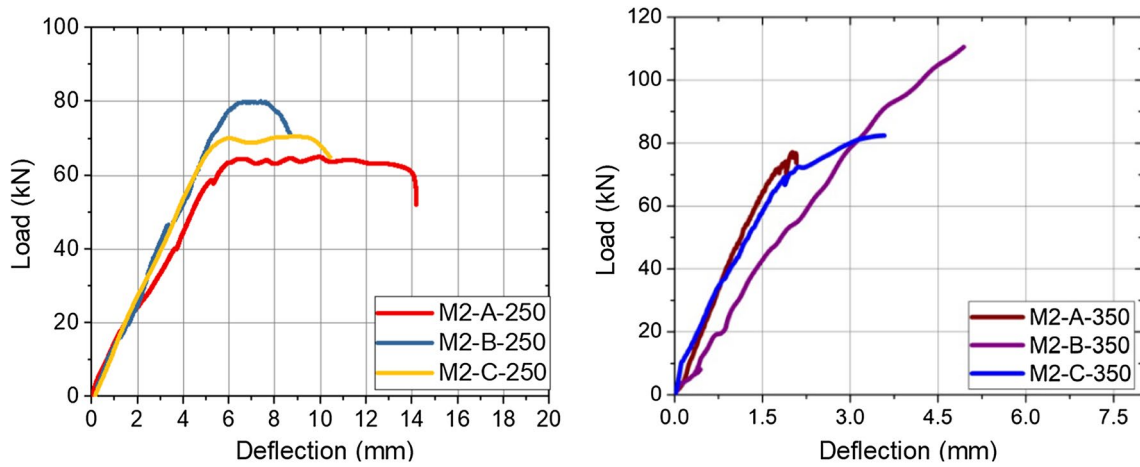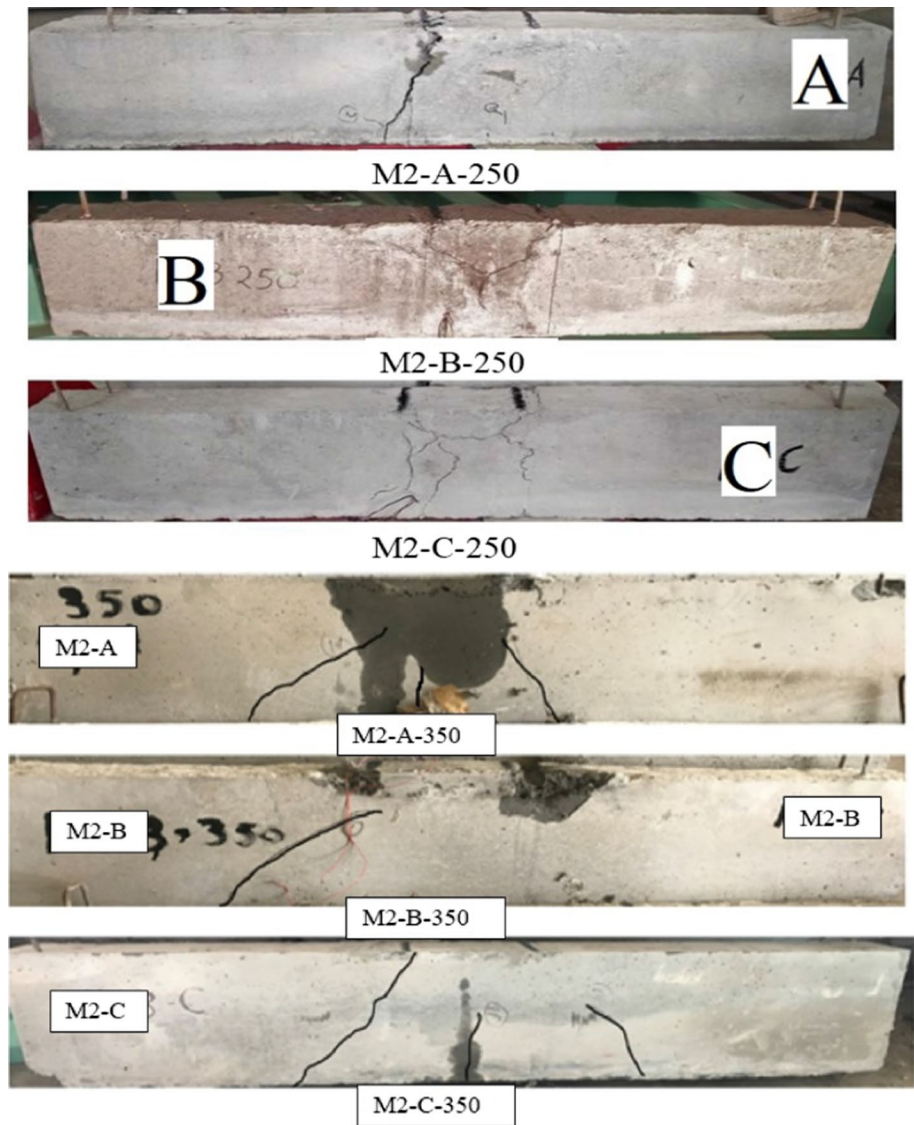M2-A-350

M2-B-350

M2-C-350

Fig. 10 Load–deflection response of test beams

For beam depths of 250 mm and 350 mm, the maximum range of deflection observed is 8–14 mm and 1.7 to 4.7 mm, respectively. It was also found that the ultimate shear carrying capacity (Vexp) also improved with an improvement in the reinforcing ratio for 350-mm-deep beams with maximum shear values of 38.94 kN, 55.26 kN, and 41.2 kN for beams M2-A-350, M2-B-350, and M2-C-350. Normalised shear values have been determined from the shear values derived from the experiments and are displayed in Table 6 for all 350-mm-deep beams.

4.2.3 Load, Reinforcement, and Concrete Strains

Figures 11 and 12, respectively, demonstrate the plot of strain in reinforcement and top surface concrete. The values obtained were evaluated only in the pure bending zone between the application load points. Positive values of strain refer to tension in reinforcement, while negative refer to compression in the top concrete surface. As the reinforcing ratio increased in all the beams, both compressive and tensile strains were increased. For the depth of 250 mm beams, Fig. 11 shows that the reinforcement strain persisted at low levels initially at lower loads applied up to 20 kN, but as the load rose above 20 kN, the reinforcement strain increased rapidly. The sudden rise in reinforcement strain confirms that the load was moved to reinforcement after 20 kN load application and distributed between steel and concrete. With more load increases, the reinforcement strain has also increased, and beyond the 62 kN and 71 kN load applications for the M2-A-250 and M2-C-250 beams, the strain values have only increased with little to no additional loads applied. These increased strain values confirm that reinforcement yields have occurred for beams M2-A-250 and M2-C-250. The reinforcement strain plot increased linearly up to 80 kN load with no reinforcement yield for beam
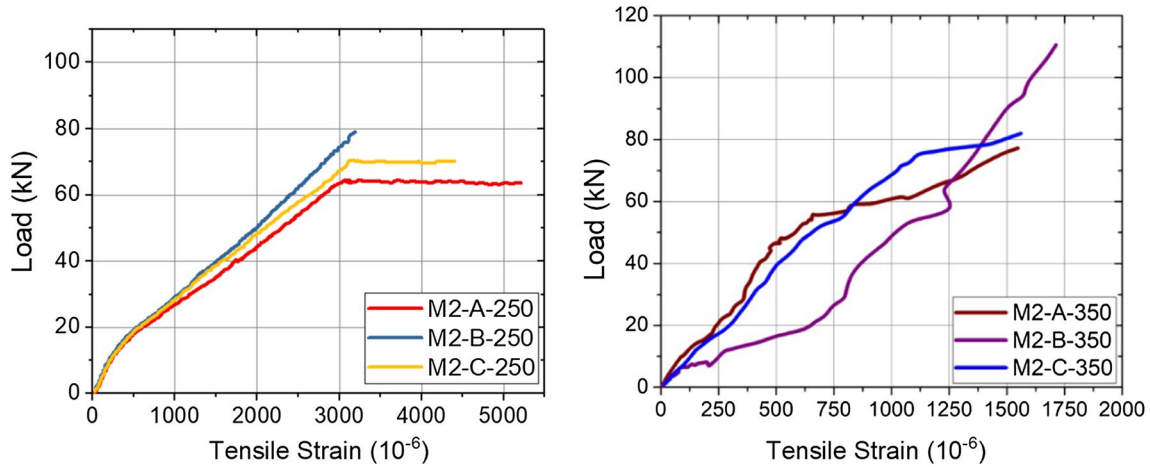

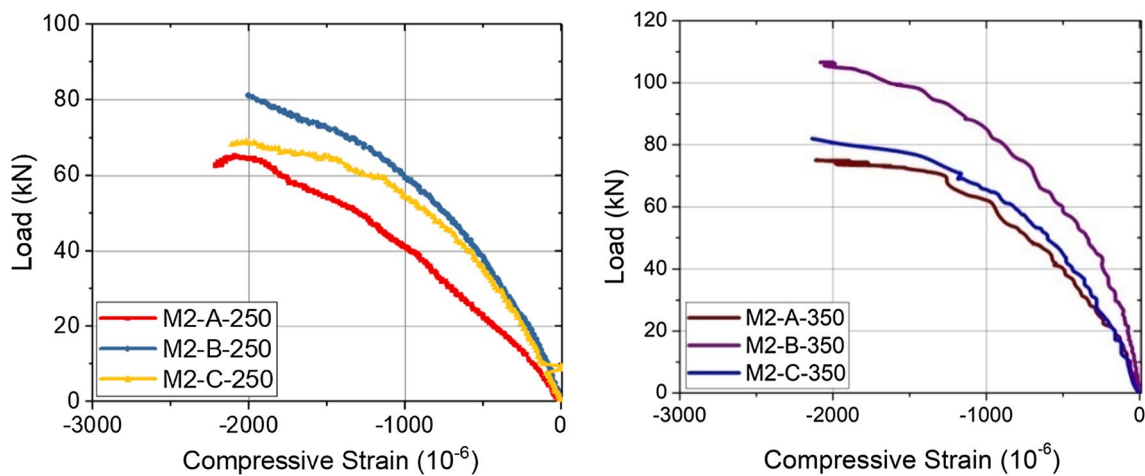**Fig. 11** Load vs strain in reinforcement

Fig. 12 Load vs compressive strain in concrete (top surface)

M2-B-250, as a failure in that beam was due to concrete crushing because of the presence of a higher reinforcement ratio.

On the other hand, the strain in reinforcement increased for 350-mm-deep beams as load increased to failure. Since all the beams failed due to shear, no reinforcement yield for any beam was found. The reinforcement plot for beam M2-B-350 had peculiar variations, which may be due to the reinforcement strain gauge's partial de-bonding. Figure 12 shows that concrete compressive strain at the top surface increased continuously with an increase in a load before failure. The same pattern in concrete strain was observed for all the beams irrespective of beam depth and reinforcement ratios.

4.2.4 Ductility

As the beams of depth 250 mm failed due to yielding of reinforcement, ductility analysis has been performed for the same beams.

Ductility is a measure of the energy absorption potential of a structural member. It can be represented as resistance to deformity while changing from the elastic region to the plastic zone's failure [39]. Ductility can be evaluated in a reinforced concrete element through any of the following techniques: (1) curvature ductility index; (2) rotational ductility index; or (3) deflection ductility index [40]. Ductility is measured using the deflection ductility index method in the current analysis. Equations (3) and (4) are used to calculate the ductility index at the ultimate load and post-cracking ductility index at cracking load.

$$\mu_u = \Delta_u / \Delta_y \tag{3}$$

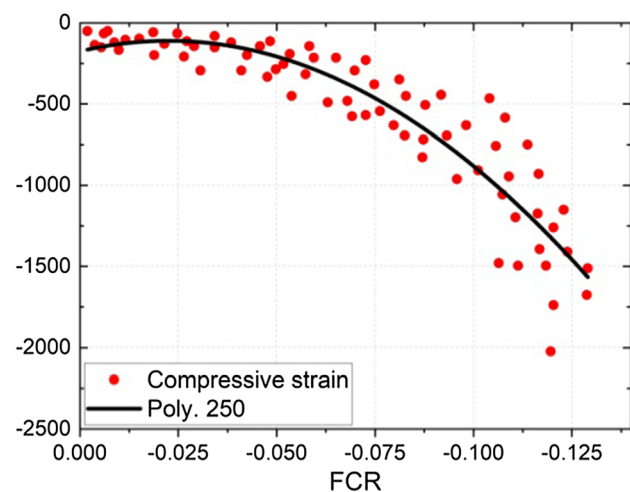$$\mu_{cr} = \Delta_u / \Delta_{cr} \tag{4}$$

Table 5 presents the summary of test results and the calculated ductility indexes for 250-mm-deep beams. From the obtained results, it was observed that, as the flexural reinforcement ratio increased, both ductility indices decreased for all the beams. The cause of the reduction in ductility index is due to the presence of a high reinforcement ratio resulting in brittle compression failure of the beam the M2-B-250 before yielding reinforcement with reduced deflection.

5 Influence of Carbon Fibres on the Relationship Between FCR and Strains

The plot of strains in concrete and steel concerning FCR values for two separate beam sets is shown in Figs. 13 and 14. The relationship between FCR and time was approximated by nominalising the curves obtained in Figs. 6 and 7. Therefore, two different relationships between FCR and strain have been obtained separately for compressive and tensile surfaces using the principle of regression analysis.

It was noticed from the findings obtained that there was a curvilinear monotonic relationship between FCR and compressive strain. In contrast, there was a linear monotonic association between FCR and tensile strain. The relationship between strain (tensile/compressive) and FCR can be expressed as

$$y = ax^2 + bx + c \tag{5}$$

In the above equation, abscissa (x) refers to FCR values, and ordinate (y) refers to stain values. Furthermore, **a**, **b** and **c** are constant parameters, the values of which are tabled in Table 7 along with values of coefficients of correlation (R^2).
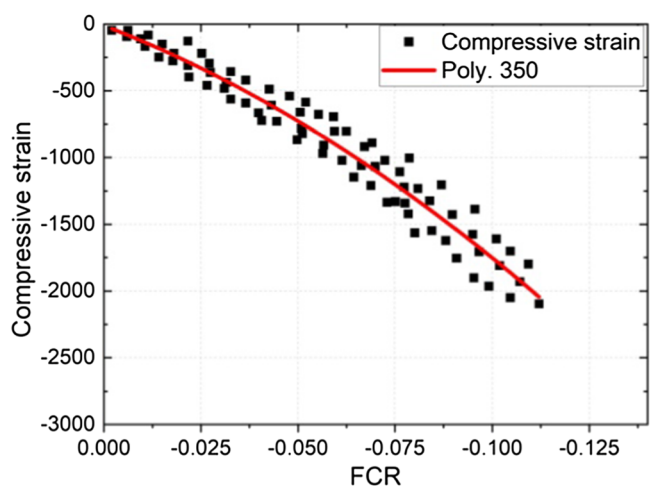

Fig. 13 Regression line drawn on scatter diagram relating FCR and Compressive strain
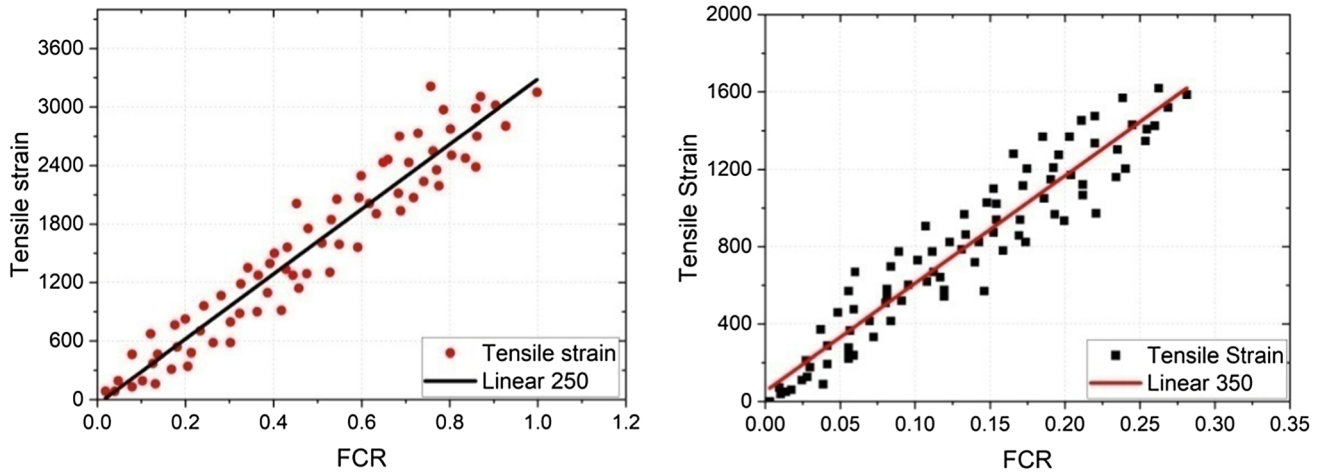
Fig. 14 Regression line drawn on scatter diagram relating FCR and tensile strain

It can be seen that the error is minimal from the R^2 values obtained, and therefore the obtained equations indicate the excellent relationship between FCR and strains. Thus if FCR is known in this case, strain (compressive/tensile) values can be obtained during loading using Eq. (5) obtained in the current study. Therefore, this technique offers a unique structural health monitoring approach to get strains/loads/stress values using smart concrete.

6 Conclusion

An experimental study on six large-scale RC beams was performed to investigate the self-sensing property of embedded smart concrete in RC beams designed to fail under shear and flexure. All the beams were tested under four-point loading that was manufactured without any shear stirrups by incorporating smart concrete in the middle portion for partial depth.

The basic structural/mechanical properties of carbon fibre-based (smart concrete) RC beam were also obtained along with self-sensing properties. Based on the experimental results, the following conclusions can be drawn:

- It is possible to effectively use RC beam fabricated with CF-based/smart concrete dosed with 1.5 percent carbon

fibre to assess the strain and crack in the reinforced concrete beam tested under four-point bending. The depth of the beam and the presence of reinforcement in differing proportions would also not impact the RC beam's self-sensing properties.

- For all the beams, the self-sensing property was obtained in the pure bending region, and FCR values were obtained either until the beam collapsed or until the embedded smart concrete developed a wider crack. In particular, smart concrete's self-sensing property showed promising results for the beams that failed to flexure by representing all the cracks formed in the pure bending region.

- Also, it was found that, as the load increases the fractional change in resistance decreases for compression surface (concrete under compression) and increases for tension surface due to the movement of carbon fibres towards and away from each other, respectively, in carbon fibre-based concrete. This phenomenon remained the same for all the beams irrespective of beam depth and reinforcement ratio.

- Out of six beams, two 250-mm-deep beams (M2-A and M2-C) failed due to reinforcement yield due to lower reinforcement ratio and one (M2-B) due to concrete crushing. Due to shear, the remaining three beams of 350 mm depth failed because of greater depth and higher

Table 7 Curve fitting parameters of the regression analysis equation

Failure type	Strain type	Correlation coefficient R^2	Constant a	Constant b	Constant c
Flexural	Compressive strain	0.84	− 12,532	− 4508	− 101.7
	Tensile strain	0.96	0	3401	141.1
Shear	Compressive strain	0.95	− 51,945	− 2204	− 61.5
	Tensile strain	0.91	0	5201	52.5

reinforcement ratio. The beam deflection and load-carrying capacity for all the beams were increased on the other side by improving the reinforcement ratio.

- An empirical relationship between FCR and strain was described differently for tension and compression surface in equation form for two different forms of failures from experimentally obtained FCR and strain values. This derived equation will help understand strain/stress/load in any instance of loading with smart concrete FCR readings, offering a new SHM technique as an NDT approach.

Funding None.

Declarations

Conflict of interest Author Arvind Kumar Cholker declares that he has no conflict of interest.

References

1. Yıldırım, G.; Sarwary, M.H.; Al-Dahawi, A.; Öztürk, O.; Anıl, Ö.; Şahmaran, M.: Piezoresistive behavior of CF- and CNT-based reinforced concrete beams subjected to static flexural loading: shear failure investigation. Constr. Build. Mater. (2018). https://doi.org/10.1016/j.conbuildmat.2018.02.124
2. Celebi, M. (2000) Seismic Instrumentation of Buildings. US Department of the Interior, US Geological Survey
3. Wang, B.S.; Ni, Y.Q.; Ko, J.M.: Damage detection utilising the artificial neural network methods to a benchmark structure. Int J Struct Eng **2**, 229–242 (2011). https://doi.org/10.1504/IJSTRUCTE.2011.040782
4. Abudayyeh, O.Y.; Barbera, J.; Abdel-Qader, I.; Cai, H.; Almaita, E.: Towards sensor-based health monitoring systems for bridge decks: A full-depth precast deck panels case study. Adv Civ Eng (2010). https://doi.org/10.1155/2010/579631
5. Leng, J.S.; Winter, D.; Barnes, R.A.; Mays, G.C.; Fernando, G.F.: Structural health monitoring of concrete cylinders using protected fibre optic sensors. Smart. Mater. Struct. (2006). https://doi.org/10.1088/0964-1726/15/2/009
6. Fraser, M.; Elgamal, A.; He, X.; Conte, J.P.: Sensor network for structural health monitoring of a highway bridge. J. Comput. Civ. Eng. (2010). https://doi.org/10.1061/(asce)cp.1943-5487.0000005
7. Han, B.; Yu, X.; Ou, J.: Self-Sensing Concrete in Smart Structures. Butterworth-Heinemann, Oxford (2014)
8. Mo, Y.L.; Howser, R.: Carbon nanofiber concrete for damage detection of infrastructure. Adv. Nanofibers. (2013). https://doi.org/10.5772/57096
9. Javier Baeza, F.; Chung, D.D.L.; Zornoza, E.; Andión, L.G.; Garcés, P.: Triple percolation in concrete reinforced with carbon fiber. ACI. Mater. J. **107**(4), 396 (2010)
10. Sathyanarayanan, K.S.; Sridharan, N.: Self sensing concrete using carbon fibre for health monitoring of structures under static loading. Indian. J. Sci. Technol. (2016). https://doi.org/10.17485/ijst/2016/v9i23/95869
11. Sobolkina, A.; Mechtcherine, V.; Khavrus, V.; Maier, D.; Mende, M.; Ritschel, M., et al.: Dispersion of carbon nanotubes and its influence on the mechanical properties of the cement matrix. Cem.

Concr. Compos. **34**, 1104–1113 (2012). https://doi.org/10.1016/j.cemconcomp.2012.07.008
12. Bandyopadhyaya, R.; Nativ-Roth, E.; Regev, O.; Yerushalmi-Rozen, R.: Stabilization of individual carbon nanotubes in aqueous solutions. Nano. Lett. (2002). https://doi.org/10.1021/nl010065f
13. Yıldırım, G.; Sarwary, M.H.; Al-Dahawi, A.; Öztürk, O.; Anıl, Ö.; Şahmaran, M.: Piezoresistive behavior of CF- and CNT-based reinforced concrete beams subjected to static flexural loading: Shear failure investigation. Constr. Build. Mater. **168**, 266–279 (2018). https://doi.org/10.1016/j.conbuildmat.2018.02.124
14. Naeem, F.; Lee, H.K.; Kim, H.K.; Nam, I.W.: Flexural stress and crack sensing capabilities of MWNT/cement composites. Compos. Struct. **175**, 86–100 (2017)
15. Wang, B.; Liu, S.; Zhu, Y.; Ge, S.: Influence of polyvinyl pyrrolidone on the dispersion of multi-walled carbon nanotubes in aqueous solution. Russ. J. Phys. Chem. A. (2014). https://doi.org/10.1134/s0036024414130020
16. D'Alessandro, A., Ubertini, F., Materazzi, A.L., Laflamme, S., Cancelli, A., Micheli, L.: Carbon cement-based sensors for dynamic monitoring of structures. In: 2016 IEEE 16th International Conference on Environment and Electrical Engineering. https://doi.org/https://doi.org/10.1109/EEEIC.2016.7555628 (2016)
17. Ding, Y.; Han, Z.; Zhang, Y.; Aguiar, J.B.: Concrete with triphasic conductive materials for self-monitoring of cracking development subjected to flexure. Compos. Struct. (2016). https://doi.org/10.1016/j.compstruct.2015.11.051
18. Ding, Y.; Chen, Z.; Han, Z.; Zhang, Y.; Pacheco-torgal, F.: Nano-carbon black and carbon fiber as conductive materials for the diagnosing of the damage of concrete beam. Constr. Build. Mater. **43**, 233–241 (2013)
19. Shi, L.; Lu, Y.; Bai, Y.: Mechanical and electrical characterisation of steel fiber and carbon black engineered cementitious composites. Procedia. Eng. **188**, 325–332 (2017). https://doi.org/10.1016/j.proeng.2017.04.491
20. Zhang, Z.; Wei, H.; Liu, Y.; Leng, J.: Self-sensing properties of smart composite based on embedded buckypaper layer. Struct. Health. Monit. (2015). https://doi.org/10.1177/1475921714568405
21. Radhika, P., Zhangfan, J., Andrei, R., Osman, E., Ozbulut, DKH.: Self-sensing cementitious composites with graphene nanoplatelets. 1–13 (2016)
22. Nanot S, Thompson NA, Kim JH, Wang X, Rice WD, Hároz EH, et al. Single-walled carbon nanotubes. In: Springer Handbook of Nanomaterials. Springer, Berlin (2013). https://doi.org/https://doi.org/10.1007/978-3-642-20595-8_4
23. Ding, S.; Dong, S.; Ashour, A.; Han, B.: Development of sensing concrete: principles, properties and its applications. J. Appl. Phys. (2019). https://doi.org/10.1063/1.5128242
24. Nasibulina, L.I.; Anoshkin, I.V.; Semencha, A.V.; Tolochko, O.V.; Malm, J.E.M.; Karppinen, M.J., et al.: Carbon nanofiber/clinker hybrid material as a highly efficient modificator of mortar mechanical properties. Mater. Phys. Mech **13**, 77–84 (2012)
25. Konsta-Gdoutos, M.S.; Aza, C.A.: Self sensing carbon nanotube (CNT) and nanofiber (CNF) cementitious composites for real time damage assessment in smart structures. Cem. Concr. Compos. (2014). https://doi.org/10.1016/j.cemconcomp.2014.07.003
26. Vaisman, L.; Marom, G.; Wagner, H.D.: Dispersions of surface-modified carbon nanotubes in water-soluble and water-insoluble polymers. Adv. Funct. Mater. **16**, 357–363 (2006). https://doi.org/10.1002/adfm.200500142
27. Chuang, W.; Geng-sheng, J.; Bing-liang, L.; Lei, P.; Ying, F.; Ni, G., et al.: Dispersion of carbon fibers and conductivity of carbon fiber-reinforced cement-based composites. Ceram. Int. (2017). https://doi.org/10.1016/j.ceramint.2017.08.041

Springer

28. Yao, W.; Li, J.; Wu, K.: Mechanical properties of hybrid fiber-reinforced concrete at low fiber volume fraction. Cem. Concr. Res. (2003). https://doi.org/10.1016/S0008-8846(02)00913-4

29. Toutanji, H.; McNeil, S.; Bayasi, Z.: Chloride permeability and impact resistance of polypropylene-fiber-reinforced silica fume concrete. Cem. Concr. Res. (1998). https://doi.org/10.1016/S0008-8846(98)00073-8

30. Yazdanbakhsh, A.; Grasley, Z.; Tyson, B.; Al-Rub, R.K.A.: Distribution of carbon nanofibers and nanotubes in cementitious composites. Transp. Res. Rec. J. Transp. Res. Board. **2142**, 89–95 (2010). https://doi.org/10.3141/2142-13

31. Wen, S.; Chung, D.D.L.: Self-sensing of flexural damage and strain in carbon fiber reinforced cement and effect of embedded steel reinforcing bars. Carbon (2006). https://doi.org/10.1016/j.carbon.2005.12.009

32. Alarifi, I.M.: Investigation the conductivity of carbon fibercomposites focusing on measurement techniquesunder dynamic and static loads. J. Mater. Res. Technol. (2019). https://doi.org/10.1016/j.jmrt.2019.08.019

33. EFNARC TEF of SCC and CS: The European guidelines for self-compacting concrete: specification, production and use. Eur. Guidel. Self. Compact. Concr. (2005). https://doi.org/10.1016/j.asoc.2010.03.008

34. Committee, A.C.I.: Self-Consolidating Concrete. American Concrete Institute Mi, USA (2007)

35. Cholker, A.K.; Tantray, M.A.: Micro carbon fiber based concrete as a strain-damage sensing material. Mater. Today. Proc. (2019). https://doi.org/10.1016/j.matpr.2019.06.629

36. Cholker, A.K.; Tantray, M.A.: Strain-sensing characteristics of self-consolidating concrete with micro-carbon fibre. Aust. J. Civ. Eng. **00**, 1–10 (2019). https://doi.org/10.1080/14488353.2019.1704206

37. Nguyen, D., Kim, D., Thai, D.: Concrete by adding low amount of discrete carbons. (2019). https://doi.org/https://doi.org/10.3390/ma12060938

38. Shoaib, A.; Lubell, A.S.; Bindiganavile, V.S.: Size effect in shear for steel fiber-reinforced concrete members without stirrups. ACI. Struct. J. **111**, 1081–1090 (2014)

39. Yang, I.H.; Joh, C.; Kim, B.S.: Structural behavior of ultra high performance concrete beams subjected to bending. Eng. Struct. (2010). https://doi.org/10.1016/j.engstruct.2010.07.017

40. Bernardo, L.F.A.; Lopes, S.M.R.: Neutral axis depth versus flexural ductility in high-strength concrete beams. J. Struct. Eng. (2004). https://doi.org/10.1061/(asce)0733-9445(2004)130:3(452)